Separation Science and Technology
Publication details, including instructions for authors and subscription information:
http://www.informaworld.com/smpp/title~content=t713708471

Adsorption of H_2, CO_2, CH_4, CO, N_2 and H_2O in Activated Carbon and Zeolite for Hydrogen Production

Filipe V. S. Lopes[a]; Carlos A. Grande[a]; Ana M. Ribeiro[a]; José M. Loureiro[a]; Oikonomopoulos Evaggelos[b]; Vladimiros Nikolakis[b]; Alírio E. Rodrigues[a]
[a] Laboratory of Separation and Reaction Engineering (LSRE) Associate Laboratory LSRE-LCM, Department of Chemical Engineering, Faculty of Engineering, University of Porto (FEUP), Porto, Portugal [b] Foundation for Research and Technology, Hellas (FORTH), Institute of Chemical Engineering and High Temperature Chemical Processes (ICE-HT), Patras, Hellas

To cite this Article Lopes, Filipe V. S. , Grande, Carlos A. , Ribeiro, Ana M. , Loureiro, José M. , Evaggelos, Oikonomopoulos , Nikolakis, Vladimiros and Rodrigues, Alírio E.(2009) 'Adsorption of H_2, CO_2, CH_4, CO, N_2 and H_2O in Activated Carbon and Zeolite for Hydrogen Production', Separation Science and Technology, 44: 5, 1045 — 1073
To link to this Article: DOI: 10.1080/01496390902729130
URL: http://dx.doi.org/10.1080/01496390902729130

Separation Science and Technology, 44: 1045–1073, 2009

ISSN: 0149-6395 print/1520-5754 online
DOI: 10.1080/01496390902729130

Taylor & Francis
Taylor & Francis Group

Adsorption of H_2, CO_2, CH_4, CO, N_2 and H_2O in Activated Carbon and Zeolite for Hydrogen Production

Filipe V. S. Lopes,[1] Carlos A. Grande,[1] Ana M. Ribeiro,[1] José M. Loureiro,[1] Oikonomopoulos Evaggelos,[2] Vladimiros Nikolakis,[2] and Alírio E. Rodrigues[1]

[1]Laboratory of Separation and Reaction Engineering (LSRE) Associate Laboratory LSRE-LCM, Department of Chemical Engineering, Faculty of Engineering, University of Porto (FEUP), Porto, Portugal
[2]Foundation for Research and Technology, Hellas (FORTH), Institute of Chemical Engineering and High Temperature Chemical Processes (ICE-HT), Patras, Hellas

Abstract: The design of a layered pressure swing adsorption unit to treat a specified off-gas stream is based on the properties of the adsorbent materials. In this work we provide adsorption equilibrium and kinetics of the pure gases in a SMR off-gas: H_2O, CO_2, CH_4, CO, N_2, and H_2 on two different adsorbents: activated carbon and zeolite. Data were measured gravimetrically at 303–343 K and 0–7 bar. Water adsorption was only measured in the activated carbon at 303 K and kinetics was evaluated by measuring a breakthrough curve with high relative humidity.

Keywords: Adsorption kinetic, adsorption equilibrium, carbon dioxide, hydrogen, pressure swing adsorption

Received 16 June 2008; accepted 20 December 2008.

Address correspondence to Alírio E. Rodrigues, Laboratory of Separation and Reaction Engineering (LSRE), Department of Chemical Engineering, Faculty of Engineering, University of Porto, s/n, Rua Dr. Roberto Frias, Porto 4200-465, Portugal. Tel.: +351 22 508 1671; Fax: +351 22 508 1674. E-mail: arodrig@fe.up.pt

INTRODUCTION

Burning fossil fuels for various human and industry activities release annually a billion tons of greenhouse gases (GHG) into the atmosphere. The countries included in the Annex B of the Kyoto protocol have to reduce the GHG emissions to avoid economic penalties. Thus, it is imperative to give high priority to CO_2 capture and sequestration and also to efficient power generation (1, 2).

Nowadays, the steam methane reforming (SMR) is the most economical route for hydrogen production (3). The hydrogen produced by SMR is frequently purified in a pressure swing adsorption (PSA) unit. To have a sustainable production of hydrogen employing natural gas (fossil fuel), a capture process would be necessary to remove the undesired by-product (CO_2) for permanent sequestration. This is the main objective of the European Research Project HY2SEPS (Hybrid Hydrogen Carbon Dioxide Separation Processes) where the PSA technology is combined with a membrane process to produce high purity H_2 (>99.99%) integrating a CO_2 capture technology (4).

The SMR reactor produces a gas mixture containing high amounts of hydrogen (70–72 mole%), 15 to 20 mole% of carbon dioxide and is saturated with water (3). In addition, this stream is contaminated with carbon monoxide and methane. If the methane employed as fuel contains nitrogen as contaminant, this gas will also be present in the off-gas of the reformer. Many different PSA process schemes have been designed, with different column arrangements, cycle scheduling and even adsorbent layer dispositions (3,5–12). It is common practice in industrial PSA units to employ layered columns containing different adsorbents (13). In this particular case, a first layer of activated carbon is used to completely remove strongly adsorbed compounds, such as H_2O and CO_2. A second layer of a zeolite material is employed to remove the light components, i.e., N_2. The removal of CH_4 and CO may differ according to the adsorbents employed, the design of the PSA and to the composition of the stream to be treated (13).

The purpose of this communication is to report experimental data of adsorption equilibrium and kinetics of the gases exiting the SMR reactor for the design of a layered PSA unit for H_2 purification. Adsorption equilibrium isotherms of pure gases (H_2O, CO_2, CH_4, CO, N_2, and H_2) on two different adsorbents, activated carbon and zeolite, were measured. Adsorption equilibrium is reported in a pressure range of 0–7 bar, at three different temperatures (303, 323, and 343 K). The measurements cover a wide range of possible operating conditions of the PSA unit to obtain hydrogen with high purity (>99.99%). Adsorption equilibrium of water was determined only in the activated carbon sample at 303 K because it

should be removed completely within the first layer of the adsorbent. Adsorption kinetics of water was measured through a breakthrough experiment with a high relative humidity.

The adsorption equilibrium data were fitted with the multisite Langmuir model. The variation of the isosteric heat of adsorption was also calculated using the Clausius–Clapeyron equation. The data reported in this paper provides all the information required for a fundamental design of a layered PSA unit for hydrogen purification.

EXPERIMENTAL

Adsorbents Characterization

The materials employed in this work are commercial extrudates of activated carbon and zeolite. The macro and microporous structure of these materials was determined by nitrogen adsorption and mercury porosimetry.

The N_2 physisorption isotherms were measured at 77 K using an Autosorb-1 physisorption-chemisorption analyser. The samples have been degassed at 573 K for at least 2 hours before each measurement. The specific surface area, the pore volume, and the pore size distribution of the samples have been calculated using the following methods: Brunauer–Emmett–Teller (BET), Langmuir, Barrer–Joyner–Halenda (BJH), V-t and Horvath–Kawazoe (HK).

The mercury porosimetry was performed using a PoreMaster 60 Porosimeter (Quantachrome). The mercury intrusion-retraction was measured over a wide range of pressures (3.5∼400,000 kPa). The pore size distribution of the zeolite sample has been calculated assuming that the pore structure is represented by a network of pores and throats. On the other hand the pore size distribution of the carbon samples was calculated assuming that the macro/mesopores are uniform cylinders.

Adsorption Equilibrium

The adsorption equilibria of pure hydrogen, carbon dioxide, methane, carbon monoxide, and nitrogen on the activated carbon and zeolite materials were measured gravimetrically at 303, 323, and 343 K. The experimental setup consists of a magnetic suspension microbalance (Rubotherm, Germany) operated in a closed system. Pressure inside the chamber was measured with a Lucas Schaevitz pressure transducer in the range of 0–7 bar. The reversibility of each isotherm was confirmed

with adsorption and desorption measurements. Degassing of the zeolite material was performed under vacuum ($<10^{-7}$ bar) at 593 K overnight while the maximum temperature for activated carbon was 423 K. The heating rate to reach these temperatures was 1 K/min. In all the experiments performed, the values obtained correspond to the excess adsorbed phase concentration (3). To perform the buoyancy corrections, we have assumed that the density of the adsorbed phase is equal to the density of the liquid at its boiling point at 1 atm (14). Employing this correction, the final equation to calculate the absolute amount adsorbed from experimental data is (15):

$$q = \frac{\Delta m + \rho_g (V_s + V_c)}{m_s M_W} \frac{\rho_\ell}{\rho_\ell - \rho_g} \tag{1}$$

where q is absolute adsorbed phase concentration, Δm is the difference of weight between one measurement and the previous one, ρ_g is the density of the gas phase, ρ_ℓ is the density of the adsorbed phase, V_s is the volume of the solid adsorbent and V_c is the volume of the cell where the adsorbent is located (plus ancillary connections), m_s is the mass of adsorbent placed in the basket of the microbalance, and M_W is the molecular weight of the gas. In order to determine the volumes that contribute to the buoyancy effect ($V_s + V_c$), a calibration with helium was performed, under the assumption that this gas is not adsorbed ($m_{ads} = V_{ads} = 0$).

Water vapor adsorption equilibrium isotherm at 303 K on the activated carbon was measured in a magnetic suspension microbalance (Rubotherm, Germany) operating in open mode with a continuous gas flow passing through the sample. The vapor was generated by flowing helium through glass bubblers filled with water. The "saturated" stream can be mixed with a second stream of pure helium before entering the balance. The composition of the inlet gas can be regulated by balancing the flow rates of these two streams. When the sample reached a constant mass, the concentration of the outlet stream was determined with a humidity sensor SHT71 (Sensirion, Switzerland).

Adsorption Kinetics

The transport kinetics, i.e., individual diffusivities of all gases were estimated by measurements of breakthrough curves. The column was placed in a chromatograph for temperature control. Thermal conductivity detector (TCD) was employed to measure the concentration of CO_2, CO, N_2, and H_2, while the concentration of methane was detected by FID (Flame

Table 1. Experimental conditions used on the measurement of the breakthrough curves of CO_2, CH_4, CO, N_2, H_2, and H_2O at 1 bar of pressure

Adsorbent	Activated carbon	Zeolite	Activated carbon
Adsorbate	CO_2, CH_4, CO, N_2, H_2		H_2O
Adsorbate partial pressure [bar]	0.005; 1*		0.0374
Mass Adsorbent $\times 10^3$ [kg]	6.3554	8.5315	2.6258
Temperatures [K]	303, 323, 343		303
Bed height [m]	0.165		0.085
Bed volume $\times 10^5$ [m^3]	1.245		0.5053
Bed porosity, ε	0.394	0.391	0.383

Adsorbent	Activated carbon	Zeolite
Type	extrudates	extrudates
Average Pellet diameter $\times 10^3$ [m]	2.35	1.70
Average pellet length $\times 10^3$ [m]	3–4	4–6
Pellet porosity, ε_p	0.566	0.503
Adsorbent density, ρ_p [kg/m^3]	842	1126
Solid density, ρ_s [kg/m^3]	1939	2267

*The adsorbate partial pressure is 1 bar for H_2; for the other gases is 0.005 bar.

Ionization Detector). Water concentration was detected with a humidity sensor SHT71 (Sensirion, Switzerland). The activation of the samples was performed heating at 1 K/min until 423 K (activated carbon) or 593 K (zeolite) and left overnight, under a continuous flow of helium. The operating conditions and the different columns employed are detailed in Table 1. Note that, in the case of hydrogen, breakthroughs were performed with the pure gas while for CO_2, CH_4, CO, and N_2, only a content of 0.5% of adsorbate diluted in helium was used. The breakthrough curve of water on activated carbon was measured at 303 K with 89% of relative humidity (see Table 1).

THEORETICAL

Adsorption Equilibrium

The multisite Langmuir model has been capable to fit correctly adsorption data of a wide variety of gases in different adsorbents (16–19). The

multisite Langmuir model (18) results in the description of adsorption equilibrium as a localized monolayer model in which each molecule occupies more than one site on a homogeneous surface. The multisite Langmuir model is represented by:

$$\left(\frac{q_i}{q_{i,max}}\right) = a_i K_i P\left[1 - \left(\frac{q_i}{q_{i,max}}\right)\right]^{a_i} \tag{2}$$

where q_i is the amount of adsorbate i in the adsorbed phase, $q_{i,\,\max}$ is the specific saturation adsorption capacity of component i, a_i is the number of neighboring sites occupied by adsorbate molecule i, K_i is the equilibrium constant of component i, and P is the pressure.

The adsorption equilibrium constant has an exponential temperature dependence given by (20):

$$K_i = K_i^{\infty} \exp\left(\frac{-\Delta H_i}{R_g T}\right) \tag{3}$$

where K_i^{∞} is the adsorption constant of component i at infinite temperature, $(-\Delta H_i)$ is the heat of adsorption of the compound i at zero coverage and R_g is the universal gas constant. This isosteric heat of adsorption $(-\Delta H_i)_q$ has logarithmic pressure dependence according to the Clausius–Clapeyron equation:

$$(-\Delta H_i) = R_g T\left(\frac{\partial \ln P_i}{\partial T}\right)_q \tag{4}$$

where the derivative has to be evaluated at constant amount adsorbed q. Plotting $\ln P_i$ versus $1/T$, the isosteric heat of adsorption can be determined through the straight line equation with a slope equal to $-\Delta H_i/(R_g T)$.

The parameters $q_{i,\max}$ and a_i of the multisite Langmuir model (18) are independent of the temperature. A site or space balance of the adsorbed phase gives:

$$a_i\ q_{i,\max} = \text{constant} \tag{5}$$

which is a requirement for thermodynamic consistency of the multisite Langmuir model for prediction of multicomponent adsorption equilibrium (20).

The fitting of the multisite Langmuir model was performed using MATLAB (The MathWorks, Inc.).

Adsorption Kinetics

The adsorption kinetics of pure gases was determined by the measurement of breakthrough curves. For the case of CO_2, CH_4, CO, and N_2, a small quantity of the gas was diluted with helium in order to reduce velocity variations within the column, operate under isothermal conditions, and avoid effects of non-linearity of the isotherm. In the case of hydrogen, a higher concentration should be employed, the reason why velocity variations

Table 2. Correlations used to estimate the diffusivity constants

Correlation	

Sum of all resistances	$\frac{\sigma^2}{2\mu_1^2} = \frac{D_{ax}}{u_i L} + \left(\frac{u_i}{L}\right)\left(\frac{\varepsilon}{1-\varepsilon}\right)\left(\frac{R_p}{2k_f} + \frac{R_p^2}{\Omega_p \varepsilon_p D_p} + \frac{r_c^2}{\Omega_c K_H D_c}\right)\left(1 + \frac{\varepsilon_p}{(1-\varepsilon_p)K_H}\right)^{-2}$
	with $K_H >> \varepsilon_p$
	activated carbon: $\Omega_p = 8$ (cylinder particles);
	$\Omega_c = 3$ (slab micropores)
	zeolite: $\Omega_p = 8$ (cylinder particles);
	$\Omega_c = 8$ (cylinder crystals)

Axial dispersion	$D_{ax} = (0.45 + 0.55\varepsilon)D_m + 0.35 R_p u_i$
Film mass transfer	$Sh = 2.0 + 1.1 Re^{0.6} Sc^{1/3}$ with $Sh = 2R_p k_f / D_m$, $\mathrm{Re} = 2\rho_g u_o R_p / \mu$ and $Sc = \mu / \rho_g D_m$
Bosanquet equation	$\frac{1}{D_p} = \tau_p \left(\frac{1}{D_m} + \frac{1}{D_k}\right)$
Chapman–Enskog equation	$D_m = \frac{1 - y_i}{\sum_{\substack{j=1 \\ j \neq i}}^{n} \frac{y_i}{D_{ij}}}$
Knudsen diffusivity (m^2/s)	$D_k = 97.0 r_p \sqrt{\frac{T}{M_W}}$ with r_p in meters
Micropore or crystal diffusivity	$\frac{D_c}{r_c^2} = \frac{D_c^0}{r_c^2} \exp\left(-\frac{E_a}{R_g T}\right)$

were observed. Note that for hydrogen, the isotherms are linear within the entire pressure range employed for the measurements.

Analyzing the breakthrough curves and according to the correlations reported in Table 2 (21, 22), the kinetic parameters in isothermal conditions

Table 3. LDF model used for diluted breakthrough prediction

Initial conditions			
Bed, macropore and micropore or crystal	$C_B\|_0 = 0$	$C\|_0 = 0$	$q\|_0 = 0$
Boundary conditions			
Bed	$C_B\|_{Feed} = C_B\|_0 - \frac{D_{ax}}{u_i}\frac{\partial C_B}{\partial z}\Big\|_0$;		$\frac{\partial C_B}{\partial z}\Big\|_L = 0$
Macropore	$\varepsilon_p D_p \frac{\partial C}{\partial R}\Big\|_{(R_p,z)} = k_f\left(C_B\|_z - C\|_{(R_p,z)}\right)$;		$\frac{\partial C}{\partial R}\Big\|_{(0,z)} = 0$
Micropore or crystal	$q\|_{(r_c,z)} = q^*\|_{r_c}$;		$\frac{\partial q}{\partial r}\Big\|_{(0,z)} = 0$

Equations

$$\frac{\partial C_B}{\partial t} + \rho_p\left(\frac{1-\varepsilon}{\varepsilon}\right)\frac{\partial\langle\bar{q}\rangle}{\partial t} + u_i\frac{\partial C_B}{\partial z} = D_{ax}\frac{\partial^2 C_B}{\partial z^2}$$

$$\langle\bar{q}\rangle = \frac{2}{R_p^2}\int_0^{R_p}\bar{q}R\,dR$$

$$\frac{\partial C}{\partial t} + \rho_p\left(\frac{1-\varepsilon_p}{\varepsilon_p}\right)\frac{\partial\langle\bar{q}\rangle}{\partial t} = D_p\frac{\partial^2 C}{\partial R^2}$$

$$q^*|_{(R,z)} = KC|_{(R,z)}$$

$$\frac{\partial q}{\partial t} = D_c\left(\frac{\partial^2 q}{\partial r^2} + \frac{2}{r_c}\frac{\partial q}{\partial r}\right)$$

$$\bar{q} = \frac{1}{r_c}\int_0^{r_c} q\,dr$$

and with almost constant flowrate were estimated. To fit the breakthrough curves it was employed the mathematical model described in Table 3 (22). The model assumes that the process is isothermal, that the velocity is constant within the column and that the adsorbent particle is bidisperse; composed of macro and micropores. The numerical solution of the mathematical model (Table 3) was performed using gPROMS (PSE Enterprise, UK) using the orthogonal collocation on finite elements (OCFEM). The number of elements used was 25 with two interior collocation points (third order polynomials) in each element of the adsorption bed. The simulations were performed with an absolute and relative tolerance of 1×10^{-5}.

RESULTS AND DISUSSION

Adsorbents Characterization

Nitrogen adsorption isotherms at 77 K for activated carbon and for zeolite are shown in Fig. 1. The results on the activated carbon sample show a high amount of micropores and only a small fraction of macropores. On the other side, the analysis of the zeolite sample shows the micropores of the zeolite crystals and a region of mesopores. The mesopores are not within the zeolite crystals but are due to the porous structure of the inert matrix used to support the crystals. The micropore size distribution (calculated using the HK method) of both samples is also represented in Fig. 1. The activated carbon sample presents a wide distribution of micropores within 6 to 15 Å. On the other side, the micropore distribution of the zeolite is much narrower with an average

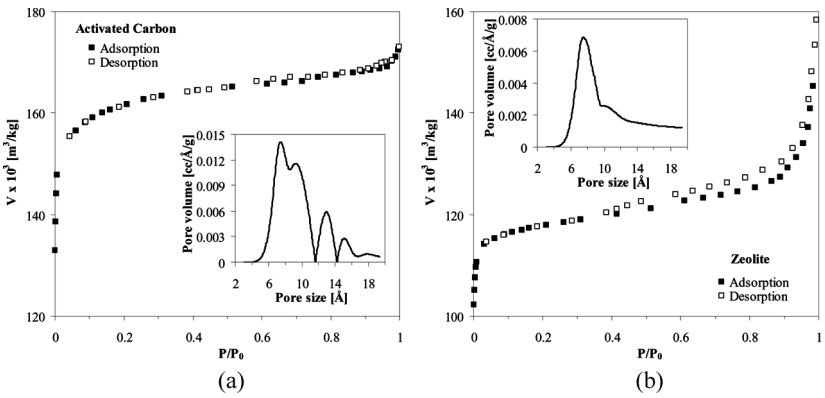

Figure 1. Nitrogen adsorption isotherm and pore size distribution calculated using the HK method for the activated carbon (a) and zeolite (b) sorbent materials.

size of 7.4 Å and a much smaller amount of 10.2 Å. The summary of the characterization values obtained with the N_2 physisorption experiment for both adsorbents is shown in Table 4.

The mercury porosimetry was performed to determine the macropore structure of the activated carbon and zeolite extrudates. The respective pore and throat size frequency distribution functions are represented in Fig. 2. The macropore distribution within the zeolite is very narrow with a very well-defined average at 4.25 μm. On the other side, the macroporous structure of the activated carbon is also widespread with macropores of several diameters. The average pore diameter distribution is 15.9 and 4.25 μm for the activated carbon and zeolite, respectively. Table 4 summarizes the data obtained in the analysis of the mercury porosimetry experiments for both adsorbent materials.

Adsorption Equilibrium of H_2, CO_2, CH_4, CO, and N_2

Adsorption equilibrium isotherms of carbon dioxide, methane, carbon monoxide, nitrogen, and hydrogen were measured at 303, 323, and 343 K in the pressure range between 0 and 7 bar. Adsorption equilibrium data are shown in Figs. 3 to 7 for each gas in the two adsorbents studied in this work. A total of thirty isotherms were measured and it was confirmed that adsorption equilibrium of all gases is reversible.

The adsorption capacity of the activated carbon is: $CO_2 > CH_4 > CO > N_2 > H_2$ while for the zeolite is $CO_2 > CO > CH_4 > N_2 > H_2$.

In the activated carbon adsorbent, the amount adsorbed of carbon dioxide (at 303 K and 7 bar) is ~4.1 mol/kg. Other samples of activated carbons show relatively higher capacities at 7 bar; i.e, ~5.4 mol/kg (23) at 293 K, ~5.8 mol/kg (2) at 296 K and ~5.9 mol/kg (24), ~6.6 mol/kg (14) and ~6.7 mol/kg (25) at 298 K. This indicates that the CO_2 adsorption of the activated carbon studied has lower capacities than the materials found in the literature. However, when the CO_2/H_2 selectivity of the activated carbon studied and the activated carbons just mentioned are compared, the results have a considerably different analysis. For the material studied, a higher selectivity of carbon dioxide-hydrogen at 303 K and 7 bar (19.7) was obtained than for the materials reported in the literature: ~17.1 (2) at 296 K and ~9.67 (24) and ~11 (25) at 298 K. Only in one case the CO_2/H_2 selectivity at 7 bar reaches such high values: ~19.3 (23) at 293 K. For the separation of the SMR off-gases, the high selectivity of the activated carbon studied is an important factor to bear in mind.

In the zeolite extrudates, the CO_2 amount adsorbed is ~4 mol/kg (at 303 K and 7 bar) with a much higher steepness than in the activated

Table 4. Specific surface areas, total pore volumes and average pore sizes of the activated carbon and zeolite samples estimated from the N_2 physisorption data and using mercury porosimetry

		Activated carbon			Zeolite		
Method		Specific surface area [m^2/g]	Pore volume [cc/g]	Average pore size [Å]	Specific surface area [m^2/g]	Pore volume [cc/g]	Average pore size [Å]
N_2 physisorption	$BET_{Multipoint}$	480.8			433.9		
	Langmuir	729.9			551.5		
	BJH	806.8	0.243	<9	417.2	0.234	<9
	V-t micropore	401.4	0.208		309.9	0.124	7–8
	V-t external	79.40			130		
	HK		0.248	7.4, 9.2, 12.95, 15.11		0.1879	7.4, 10.2
	Mercury porosimetry	5.37	0.424	$d1 < 10$ $d2 \sim 30$ $d3 \sim 1 \times 10^3$	13.04	0.259	$d1 \sim 60$ $d2 \sim 1 \times 10^4$ $d3 \sim 1 \times 10^5$

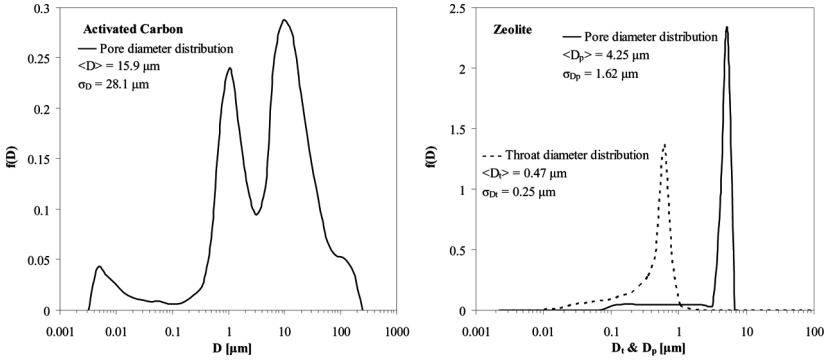

Figure 2. Pore (—) and throat (- - -) size frequency distribution functions of the activated carbon (a) and zeolite (b).

carbon sample. The data obtained in this work is similar to previously reported values of zeolite 4A and it is slightly lower than for zeolite 13X at 298 K (~4.5 mol/kg) (25). Other three samples of zeolite 13X showed higher capacities at 298 K and 7 bar: ~5.4 and ~5.7 mol/kg (24) and ~5.0 mol/kg (26).

Adsorption equilibrium of methane on the activated carbon sample (at 303 K, 7 bar) is ~2.4 mol/kg. At the same conditions, the CH_4 amount adsorbed on the zeolite sample is ~1.8 mol/kg. For carbon monoxide, the CO amount adsorbed on the activated carbon sample is ~2.0 mol/kg (at 303 K and 7 bar) and on the zeolite sample is ~2.1 mol/kg at the same conditions. Although the loading at high pressures is close, the capacity at low partial pressures is considerably larger for the zeolite. The absolute amounts adsorbed of nitrogen on the two adsorbents at 303 K and 7 bar are ~1.2 mol/kg. This is the less adsorbed gas and will be the first contaminant to breakthrough in the PSA column.

Hydrogen is the less adsorbed compound on both adsorbents. In the activated carbon sample, the amount adsorbed at 303 K for hydrogen is ~0.2 mol/kg (at 7 bar). The adsorption equilibrium capacities of hydrogen on other samples of activated carbons show results from ~0.1 mol/kg (27) to ~0.6 mol/kg (24, 25), increasing when the surface area of the adsorbent increases. At the same conditions (303 K, 7 bar), the H_2 amount adsorbed for the zeolite sample is ~0.1 mol/kg. For comparison purposes, in the literature are reported higher adsorption equilibrium capacities of hydrogen on other samples of zeolites at the same conditions, i.e, ~0.2 mol/kg (24, 25).

The adsorption equilibrium data of all the gases in the activated carbon and in the zeolite were fitted using the multisite Langmuir model

of Nitta (solid lines in Figs. 3 to 7). The parameters obtained for all gases are presented in Table 5. The model was able to fit with reasonable accuracy the data within the temperature and pressure ranges studied for the five different pure gases on both adsorbent materials studied. From the fitting parameters shown in Table 5 it can be observed that the heat of adsorption of CO_2 is much higher than the other gases for both adsorbents. The heat of adsorption of the different compounds in both adsorbents follows the same order as the adsorption capacities (activated carbon: $CO_2 > CH_4 > CO > N_2 > H_2$ and zeolite: $CO_2 > CO > CH_4 > N_2 > H_2$). The variation of the single-component isosteric heat of adsorption was calculated using the Clausius-Clapeyron equation (Fig. 8). These results are in agreement with the values obtained through the multisite Langmuir model of Nitta.

The properties exhibited by the activated carbon material (CO_2 capacity and regenerability and water tolerance) indicate that this adsorbent should be employed as the first adsorbent in a layered PSA configuration. Within this adsorbent, water will be preferentially removed and methane and carbon monoxide will also be adsorbed. The second layer of zeolite will remove the remaining CH_4, CO, and N_2. According to the higher steepness of the CO_2 isotherms in the zeolite adsorbent, it is important that all CO_2 should be removed within the activated carbon layer. Applying a second layer of zeolite in the PSA column, the N_2 adsorption capacity of the bed will increase; the capacity of the activated carbon at 1 bar (303 K) is ~0.29 mol/kg while the capacity in the zeolite is ~0.35 mol/kg. Also, considering that the density of the zeolite is higher,

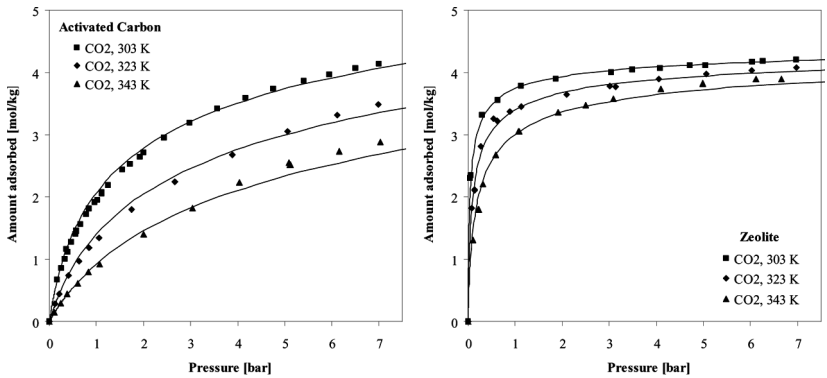

(a) (b)

Figure 3. Amount of CO_2 adsorbed on activated carbon (a) and on zeolite (b) experimental points at 303 (■), 323 (◆) and 343 K (▲) and——multisite Langmuir isotherm fitting.

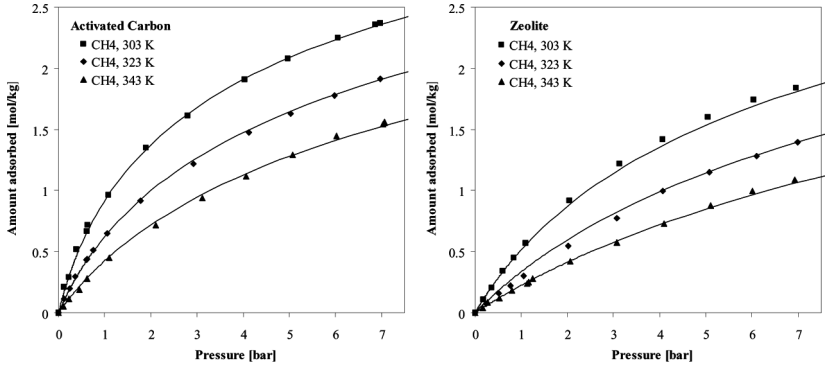

(a) (b)

Figure 4. Amount of CH_4 adsorbed on activated carbon (a) and on zeolite (b) experimental points at 303 (■), 323 (◆) and 343 K (▲) and —— multisite Langmuir isotherm fitting.

more adsorbent could be packed in a fixed volume of column, improving the process productivity.

Adsorption Kinetics of H_2, CO_2, CH_4, CO, and N_2

Adsorption kinetics of all gases were determined by breakthrough curves. In the case of CO_2, CH_4, CO, and N_2, the experiments were performed

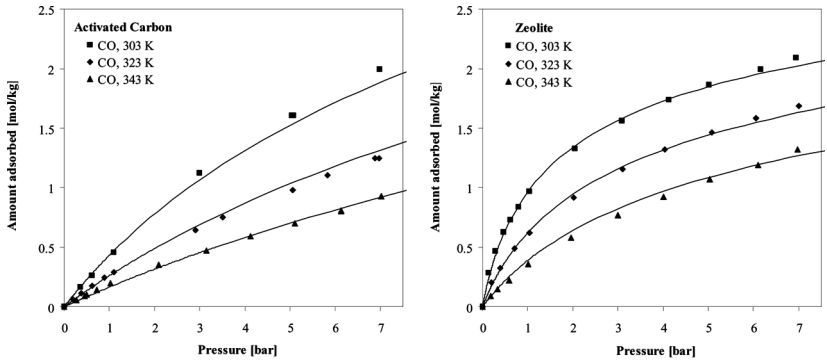

(a) (b)

Figure 5. Amount of CO adsorbed on activated carbon (a) and on zeolite (b) experimental points at 303 (■), 323 (◆) and 343 K (▲) and —— multisite Langmuir isotherm fitting.

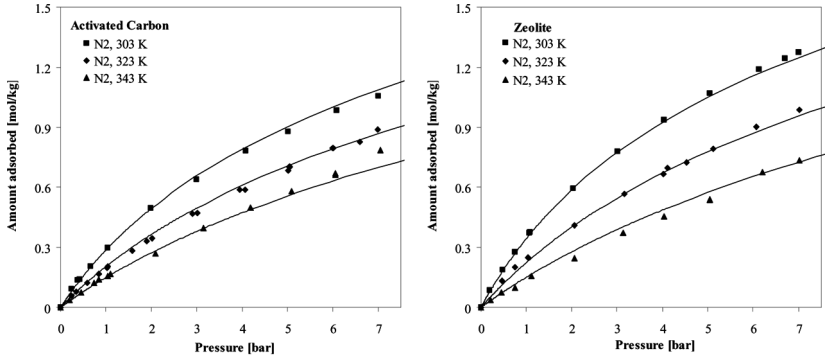

(a) (b)

Figure 6. Amount of N_2 adsorbed on activated carbon (a) and on zeolite (b) experimental points at 303 (■), 323 (◆) and 343 K (▲) and —— multisite Langmuir isotherm fitting.

using a small amount of the gas diluted in helium (see Table 1 for detailed experimental conditions). The breakthrough curves obtained for these gases are shown in Figs. 9 to 12 (carbon dioxide, methane, carbon monoxide, and nitrogen, respectively). The solid lines in all the figures correspond to the simulations using the mathematical model reported in Table 3.

Breakthrough curves of hydrogen on both adsorbents were performed using pure hydrogen. The reason for using pure hydrogen

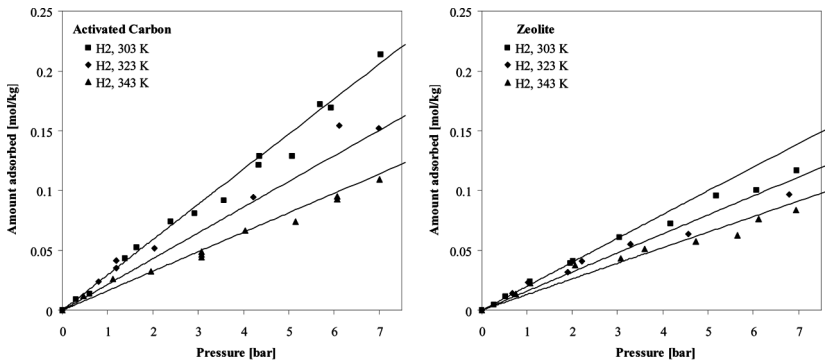

(a) (b)

Figure 7. Amount of H_2 adsorbed on activated carbon (a) and on zeolite (b) experimental points at 303 (■), 323 (◆) and 343 K (▲) and —— multisite Langmuir isotherm fitting.

Table 5. Fitting parameters of the multisite Langmuir model of Nitta for CO_2, H_2, CH_4, CO, and N_2 adsorption equilibrium on activated carbon and zeolite at 303, 323 and 343 K

Adsorbent	Gas	q_{max} [mol/kg]	a_i [–]	$K_i^{\infty} \times 10^8$ [kPa^{-1}]	$(-\Delta H)$ [kJ/mol]
Activated carbon	CO_2	7.855	3.0	2.1278	29.1
	H_2	23.57	1.0	7.6902	12.8
	CH_4	6.733	3.5	7.9165	22.7
	CO	9.063	2.6	2.6801	22.6
	N_2	5.891	4.0	23.428	16.3
Zeolite	CO_2	4.525	2.2	11.121	36.0
	H_2	9.954	1.0	52.024	9.23
	CH_4	4.976	2.0	17.793	20.6
	CO	3.828	2.6	1.5164	29.8
	N_2	4.148	2.4	12.851	20.4

breakthrough curves is because H_2 is weakly adsorbed at low partial pressures and also due to the extremely fast H_2 diffusion. The breakthrough curves of pure hydrogen on both adsorbents are reported in Fig. 13. The experimental conditions are detailed in Table 1.

The breakthrough curves present several resistances to mass transfer: axial dispersion, film in the outer layer of the extrudates, macropore diffusion, and micropore diffusion. To employ these breakthrough curve experiments to fit the diffusivity parameters, the axial dispersion and film

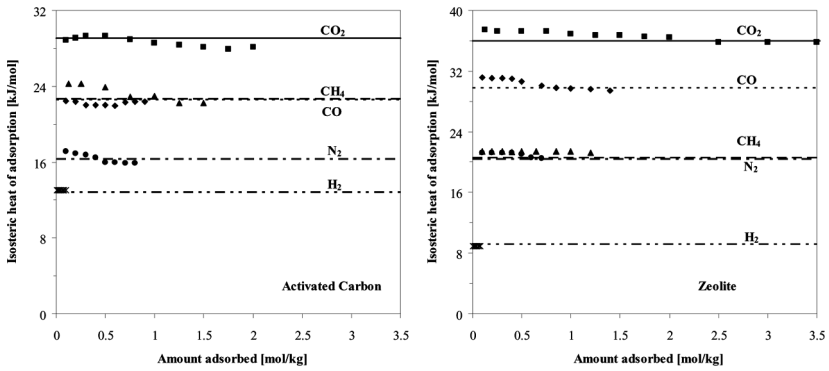

Figure 8. Single-component isosteric heats of adsorption on activated carbon (a) and on zeolite (b) for CO_2 (■), CH_4 (▲), CO (◆), N_2 (●) and H_2 (*) as a function of equilibrium pressure in the temperature range of 303–343 K; Lines are the values obtained through the multisite Langmuir model of Nitta.

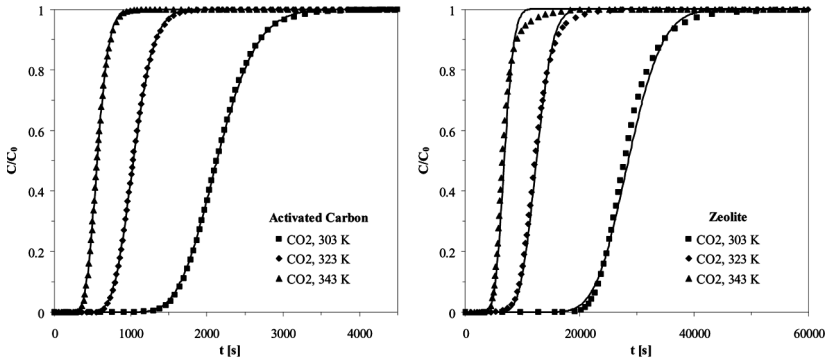

(a) (b)

Figure 9. Diluted breakthrough curves of CO_2 on activated carbon (a) and on zeolite (b) at 303 (■), 323 (◆) and 343 K (▲); 1 bar of total pressure; —— simulation with the kinetic parameters obtained; experimental conditions are detailed in Table 1.

mass transfer were estimated. According to the values from the mercury porosimetry, the pore radius of the macropore structure was large enough to neglect Knudsen diffusion (larger than the mean molecular path: e.g., for CO_2 at 297 K and 0.4–2.8 bar is 314–116 Å (28)), reason why pore diffusion was only calculated using molecular diffusion (11).

To determine the relative importance of all the resistances, the moment analysis was performed and the results obtained are reported

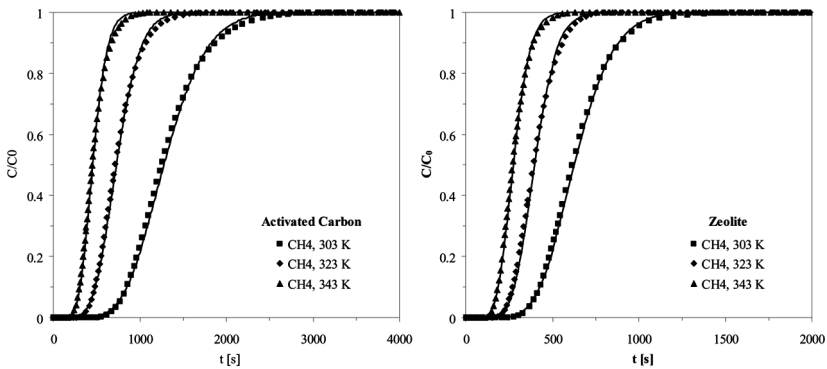

(a) (b)

Figure 10. Diluted breakthrough curves of CH_4 on activated carbon (a) and on zeolite (b) at 303 (■), 323 (◆) and 343 K (▲); 1 bar of total pressure; —— simulation with the kinetic parameters obtained; experimental conditions are detailed in Table 1.

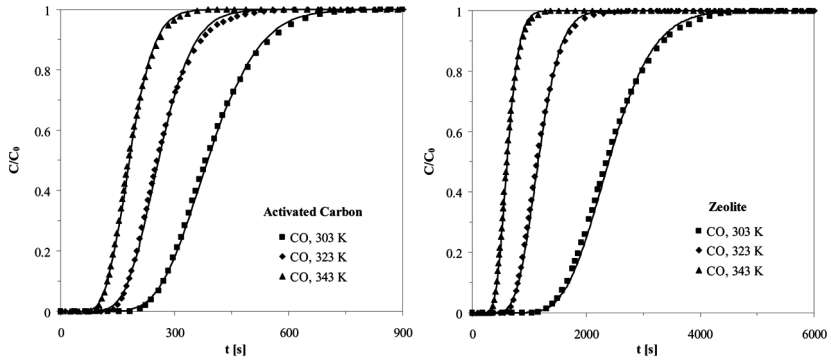

Figure 11. Diluted breakthrough curves of CO on activated carbon (a) and on zeolite (b) at 303 (■), 323 (◆) and 343 K (▲); 1 bar of total pressure; —— simulation with the kinetic parameters obtained; experimental conditions are detailed in Table 1.

as additional information in Appendix section (Tables A1 and A2). Using the derivative of the breakthrough curves, the first moment gives us the capacity of the adsorbent and the second moment is the sum of all the resistances to mass transfer. At the experimental conditions employed it was observed that the film mass transfer resistance can be neglected having a very small effect. Assuming a tortuosity value of 2 it was also observed that the macropore resistance was smaller than 3% in all

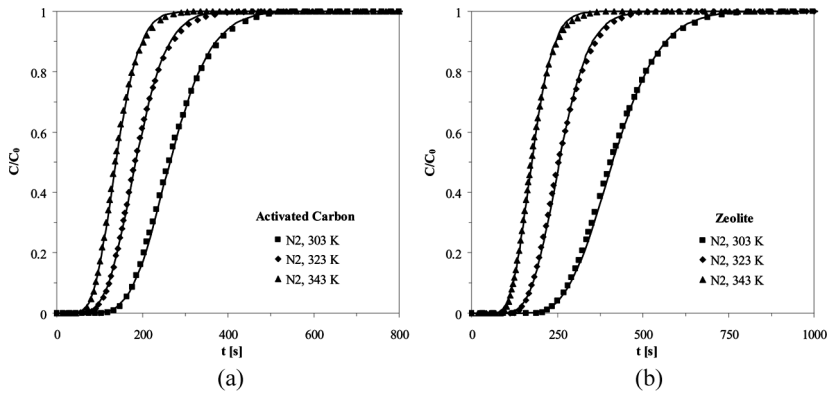

Figure 12. Diluted breakthrough curves of N_2 on activated carbon (a) and on zeolite (b) at 303 (■), 323 (◆) and 343 K (▲); 1 bar of total pressure; —— simulation with the kinetic parameters obtained; experimental conditions are detailed in Table 1.

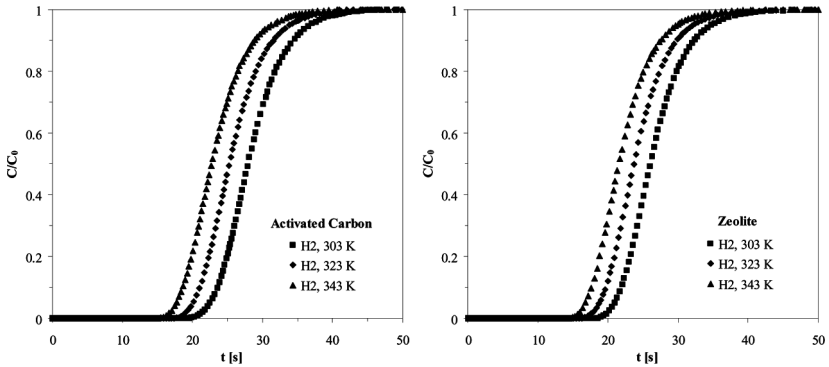

Figure 13. Breakthrough curves of H_2 on activated carbon (a) and on zeolite (b) at 303 (■), 323 (◆) and 343 K (▲); 1 bar of total pressure; experimental conditions are detailed in Table 1.

the cases (Tables A1 and A2). In all the breakthrough curves, the important dispersive mechanisms were the axial dispersion and also the micropore mass transfer resistance. The axial dispersion was estimated using the equation given in Table 2 (valid for low Reynolds numbers) and depends on the molecular diffusion and also on the velocity employed in the experiments. We have concluded that in the activated carbon and zeolite extrudates (bidisperse adsorbents), the controlling resistance to mass transfer of all gases within the particles is the micropore or crystal diffusion.

The micropore diffusion was thus estimated using the second moment calculated from the derivatives of the breakthrough curves. The specific values obtained from all the derivatives of the breakthrough curves and the exponential dependence with temperature of micropore diffusion are detailed in Table 6. It can be observed that in both adsorbents hydrogen (the smaller molecule) is the one where a higher diffusion rate is observed. The diffusion of the whole set of molecules follows the trend that can be predicted from the molecular diameters of the molecules: larger molecules have smaller diffusion coefficients. As an example, the macropore diffusivities of the five gases for the activated carbon at 303 K are: 7.21×10^{-5} (H_2)>3.55×10^{-5} (CO)>3.49×10^{-5} (N_2)>3.42×10^{-5} (CH_4)>2.91×10^{-5} m^2/s(CO_2). However, since $D_c \sim D_p/K$, the micropore diffusivities have dependence not only of the macropore diffusivity but also of the slope of the isotherm. Reason why for the activated carbon at 303 K the micropore diffusivity have the following order: 2.31×10^{-1} (H_2) >6.44×10^{-2} (N_2) >5.79×10^{-2} (CO) >3.35×10^{-2} (CO_2) >9.41×10^{-3} s^{-1} (CH_4).

Table 6. Micropore or crystal diffusivity (divided by r_c^2) and the parameters to describe temperature dependence of micropore or crystal diffusion of CO_2, H_2, CH_4, CO, and N_2 in the activated carbon and zeolite within 303–343 K at infinite dilution

		Activated carbon		Zeolite	
Gas	T [K]	D_c/r_c^2 [s^{-1}]	D_c^0/r_c^2 [s^{-1}]; E_a [kJ/mol]	D_c/r_c^2 [s^{-1}]	D_c^0/r_c^2 [s^{-1}]; E_a [kJ/mol]
CO_2	303	3.35×10^{-2}	17.5; 15.8	6.40×10^{-4}	0.268; 18.0
	323	4.74×10^{-2}		9.70×10^{-4}	
	343	6.97×10^{-2}		1.47×10^{-3}	
H_2	303	2.31×10^{-1}	14.8; 10.4	9.32×10^{-2}	9.33; 11.6
	323	3.17×10^{-1}		1.20×10^{-1}	
	343	3.73×10^{-1}		1.60×10^{-1}	
CH_4	303	9.41×10^{-3}	81.5; 22.8	9.46×10^{-3}	36.9; 20.6
	323	1.64×10^{-3}		2.12×10^{-2}	
	343	2.71×10^{-2}		2.42×10^{-2}	
CO	303	5.79×10^{-2}	59.2; 17.5	4.38×10^{-3}	368; 28.7
	323	8.08×10^{-2}		7.88×10^{-3}	
	343	1.31×10^{-1}		1.66×10^{-2}	
N_2	303	6.44×10^{-2}	0.995; 7.03	2.11×10^{-2}	7.86; 14.9
	323	6.47×10^{-2}		3.12×10^{-2}	
	343	8.98×10^{-2}		4.20×10^{-2}	

Several studies have determined diffusion constants of these gases in activated carbons and zeolites. Most of the data is expressed as LDF (linear driving force) coefficients (K_{LDF}) which correspond to $K_{LDF} = 3D_c/r_c^2$ for activated carbons and $K_{LDF} = 8D_c/r_c^2$ for zeolites. In this study, the LDF coefficients of CO_2 ($\sim 0.1\,s^{-1}$), H_2 ($\sim 0.7\,s^{-1}$), CO ($\sim 0.17\,s^{-1}$) and N_2 ($\sim 0.19\,s^{-1}$) are of the same order of magnitude of the values reported by Park and co-workers (13) and Jee and co-workers (29). However, the same authors presented a LDF coefficient of CH_4 for activated carbon much higher than the value obtained in the present work; the result obtained is $\sim 0.03\,s^{-1}$ and in the literature are reported $\sim 0.195\,s^{-1}$ (29) and $\sim 0.4\,s^{-1}$ (13). Warmuziński and Tańczyk (30) reported a LDF coefficient of CH_4 of $\sim 0.068\,s^{-1}$ (the same order of magnitude of the value obtained in this study). The LDF coefficients for zeolite materials are reported by the same authors. These coefficients of H_2 ($\sim 0.7\,s^{-1}$), CO ($\sim 0.03\,s^{-1}$) and N_2 ($\sim 0.17\,s^{-1}$) for zeolite are in agreement with the values reported (13, 29). The LDF coefficient of CH_4 for zeolite is $\sim 0.08\,s^{-1}$ and it is two times smaller than $\sim 0.14\,s^{-1}$ (29) or $\sim 0.2\,s^{-1}$ (13). The difference in the results with the literature indicates the specific interactions of the CH_4 molecules with the surface of both adsorbent materials.

Water Adsorption

The off-gases of a steam reformer contain large amounts of water. Normally before the PSA unit there exists a water separator, but the exiting stream is still saturated with water at the exit temperature. There are several approaches to remove water. Some processes use a separate unit containing normally alumina and other adsorbents to remove water before the H_2 PSA unit (11). The other possibility is to remove water in the same unit, either by using alumina as a selective adsorbent (5, 6) or by removing it in the initial layer of activated carbon (8). To evaluate this last possibility, the adsorption equilibrium of water on the activated carbon sample was measured at 303 K. The adsorption equilibrium isotherm is presented in Fig. 14. It should be noted that each point of this isotherm took around one day to reach equilibrium. The isotherm is Type V (IUPAC classification) and is characterized by an initial unfavorable region followed by a steeper region and then a final plateau. It has to be noted that the amount of water adsorbed in the activated carbon is much higher than the other gases, the reason being that it is the most adsorbed compound: ~12 mol/kg at 303 K and with a saturation pressure of 0.042 bar. Besides, the initial unfavorable region of the adsorption

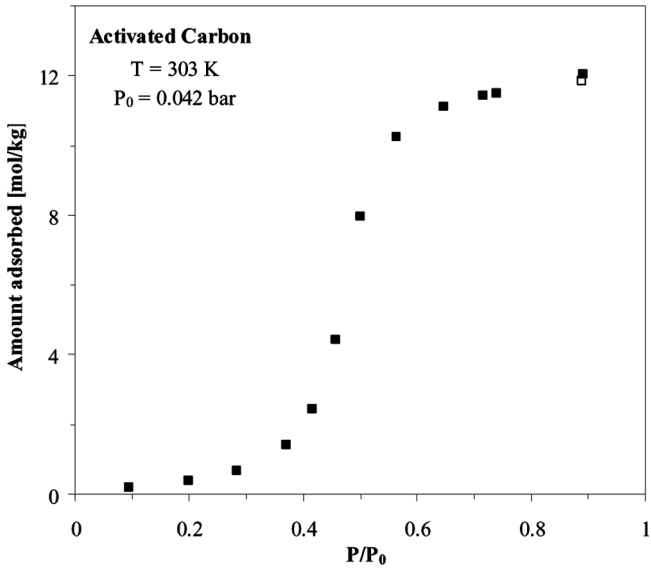

Figure 14. Amount of H_2O adsorbed on activated carbon at 303 K (■); open symbol (□) obtained from the analysis of the breakthrough experiment; experimental conditions are detailed in Table 1.

isotherm makes the regeneration of the activated carbon easier. Although it was not measured, the adsorption of water in the zeolite material should be avoided because it is very strong and the adsorbent should be regenerated at high temperatures. Sircar and co-workers (31) reported the difficult water desorption from the zeolite (even at very low partial pressures), becoming a very energy intensive process.

A water vapor breakthrough experiment in the activated carbon extrudates was also performed at 303 K using an inlet humidity percentage of 89%. The exit concentration as a function of time is reported in Fig. 15. The obtained breakthrough curve is composed of two parts as a result of the shape of the isotherm. The first part is dispersive as a result of the unfavorable part of the isotherm and the second part is a compressive front or shock that results from the second portion of the isotherm. In this second part of the breakthrough curve, a steep rise in the outlet concentration is observed, indicating that the dispersive effects are small, that is, that mass transfer resistances are low. One of the advantages of using activated carbon is that during the regeneration of the adsorbent at low pressures, the concentration front becomes compressive and the water vapor removal is favorable.

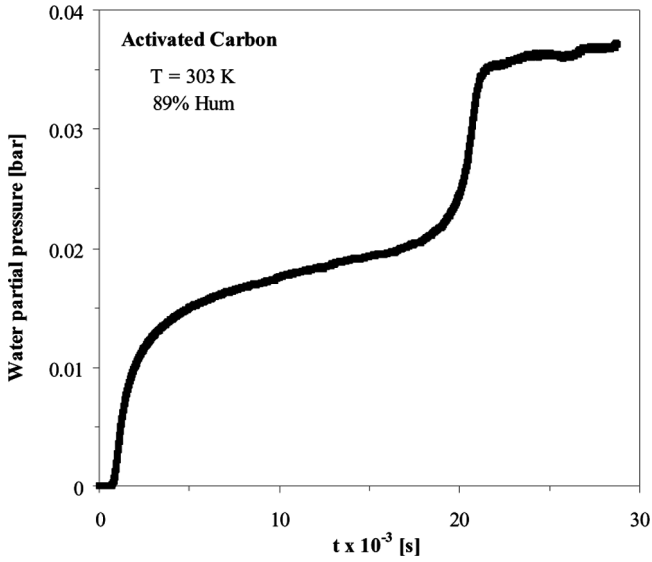

Figure 15. Water vapor breakthrough curve on activated carbon at 303 K (■) obtained with activated carbon for 89% of humidity; experimental conditions are detailed in Table 1.

CONCLUSIONS

In this work we have provided adsorption equilibrium and kinetics of the gases exiting a methane reformer. The data reported in this manuscript allows the detailed design and simulation of a layered PSA unit for hydrogen purification. Adsorption equilibrium of H_2, CO_2, CH_4, CO, and N_2 was measured at 303, 323, and 343 K between 0–7 bar in two different adsorbents: activated carbon and zeolite extrudates. These conditions are in accordance with a plant already under operation for the H_2/CO_2 separation (4) but also cover a wide range of operating conditions of the PSA unit to reach a hydrogen stream with purity higher than 99.99%. The multisite Langmuir model of Nitta was employed to fit the experimental data of H_2, CO_2, CH_4, CO, and N_2 on both adsorbent materials. It was found that this model could describe the adsorption isotherms in the whole temperature and pressure ranges studied.

Adsorption equilibrium and kinetics of water in the activated carbon adsorbent are also reported. The curve showed an initial dispersive part followed by a compressive shock indicating that regeneration of the adsorbent may be favorable. Water vapor is the most adsorbed compound in the activated carbon adsorbent indicating that this compound will be firstly removed, followed by carbon dioxide and methane. Carbon monoxide and nitrogen will be removed in the zeolite layer although the adsorption of nitrogen in the zeolite sample should be improved to make a significant difference.

The following orders of adsorption (from the most adsorbed compound to the less adsorbed gas) $H_2O > CO_2 > CH_4 > CO > N_2 > H_2$ and $CO_2 > CO > CH_4 > N_2 > H_2$ were observed in this sample of activated carbon and in the sample of zeolite, respectively. When the single-component isosteric heats of adsorption obtained through the Clausius-Clapeyron equation are compared with the correspondent values obtained by the multisite Langmuir model of Nitta, no significant discrepancies were observed. The isosteric heats of adsorption obtained through the multisite Langmuir model of Nitta are: for the activated carbon 29.1 (CO_2), 12.8 (H_2), 22.7 (CH_4), 22.6 (CO) and 16.3 kJ/mol (N_2); for the zeolite 36.0 (CO_2), 9.23 (H_2), 20.6 (CH_4), 29.8 (CO) and 20.4 kJ/mol (N_2).

Adsorption kinetic experiments of H_2, CO_2, CH_4, CO, and N_2 in the same temperature range were also performed indicating that in all cases, the mechanism controlling mass transfer is micropore diffusion. The micropore diffusivities in activated carbon of all five gases at 303 K differ in one order of magnitude having the following order from the fastest to the slowest species: $H_2 > N_2 > CO > CO_2 > CH_4$. In the case of zeolite, the values of the crystal diffusivity vary two orders of magnitude and with a diffusivity order of $H_2 > N_2 > CH_4 > CO > CO_2$ (from the fastest to the slowest gas).

ACKNOWLEDGMENT

The authors would like to thank the European Project HY2SEPS (Hybrid Hydrogen – Carbon Dioxide Separation Systems), contract No 019887, for financial support.

APPENDIX

The contribution of the axial dispersion term, film mass transfer term, pore resistance term and micropore/crystal resistance term for carbon dioxide, hydrogen, methane, carbon monoxide and nitrogen in both adsorbents are reported in Tables A1 and A2.

Table A1. Contributions of the axial dispersion term, film mass transfer term, pore resistance term and micropore resistance term for CO_2, H_2, CH_4, CO, and N_2 in activated carbon at 303, 323 and 343 K

		Term contribution [%]			
Gas	Temp. [K]	Axial disp.	Film M.T.	Pore res.	Microp. res.
CO_2	303	69.9	2.7	2.8	24.6
	323	64.3	2.2	2.4	31.1
	343	60.6	1.9	2.0	35.5
H_2	303	72.76	0.05	0.05	27.14
	323	78.54	0.03	0.03	21.40
	343	81.48	0.03	0.03	18.46
CH_4	303	45.4	0.6	0.6	53.4
	323	46.6	0.5	0.5	52.4
	343	48.6	0.5	0.5	50.4
CO	303	60.4	0.6	0.7	38.3
	323	55.3	0.5	0.5	43.7
	343	59.5	0.5	0.5	39.5
N_2	303	55.1	0.6	0.6	43.7
	323	47.7	0.4	0.4	51.5
	343	51.3	0.4	0.4	47.9

$$\frac{\sigma^2}{2\mu_1^2} = \left\{ \begin{matrix} \text{Axial} \\ \text{Disp.} \end{matrix} \right\} + \left(\frac{u_i}{L}\right)\left(\frac{\varepsilon}{1-\varepsilon}\right)\left(\left\{ \begin{matrix} \text{Film} \\ \text{M.T.} \end{matrix} \right\} + \left\{ \begin{matrix} \text{Pore} \\ \text{Res.} \end{matrix} \right\} + \left\{ \begin{matrix} \text{Microp.} \\ \text{Resist.} \end{matrix} \right\}\right) \times \left(1 + \frac{\varepsilon_p}{(1-\varepsilon_p)K_H}\right)^{-2}$$

Table A2. Contributions of the axial dispersion term, film mass transfer term, pore resistance term and crystal resistance term for CO_2, H_2, CH_4, CO, and N_2 in zeolite at 303, 323 and 343 K

		Term contribution [%]			
Gas	Temp. [K]	Axial disp.	Film M.T.	Pore res.	Microp. res.
CO_2	303	33.2	4.6	6.5	55.7
	323	29.3	3.8	5.4	61.5
	343	24.9	3.1	4.3	67.7
H_2	303	73.68	0.02	0.03	26.27
	323	78.18	0.02	0.02	21.78
	343	82.74	0.02	0.02	17.22
CH_4	303	49.1	0.3	0.4	50.2
	323	58.4	0.3	0.4	40.9
	343	52.8	0.3	0.3	46.6
CO	303	58.4	0.4	0.4	40.8
	323	56.5	0.3	0.4	42.8
	343	60.6	0.3	0.4	38.7
N_2	303	60.0	0.4	0.4	39.2
	323	59.7	0.3	0.4	39.6
	343	58.8	0.3	0.3	40.6

$$\frac{\sigma^2}{2\mu_1^2} = \left\{ \begin{matrix} \text{Axial} \\ \text{Disp.} \end{matrix} \right\} + \left(\frac{u_i}{L}\right)\left(\frac{\varepsilon}{1-\varepsilon}\right)\left(\left\{ \begin{matrix} \text{Film} \\ \text{M.T.} \end{matrix} \right\} + \left\{ \begin{matrix} \text{Pore} \\ \text{Res.} \end{matrix} \right\} + \left\{ \begin{matrix} \text{Crystal} \\ \text{Resist.} \end{matrix} \right\} \right) \times \left(1 + \frac{\varepsilon_p}{(1-\varepsilon_p)K_H}\right)^{-2}$$

NOTATION

Nomenclature

a_i number of neighbouring sites occupied by adsorbate i molecule
c concentration (mol/kg)
C bulk molar concentration in the pores of the adsorbent (mol/kg)
C_B bulk molar concentration in the gas phase (mol/kg)
D_{ax} axial dispersion coefficient (m^2/s)
D_c micropore/crystal diffusivity (m^2/s)
D_c^0 limiting diffusivity at infinite temperatures (m^2/s)

D_{ij}	binary molecular diffusivity (m^2/s)
D_m	molecular diffusivity (m^2/s)
D_p	macropore diffusivity (m^2/s)
D_k	Knudsen diffusivity (m^2/s)
E_a	activation energy of micropore diffusion (kJ/mol)
k_f	film mass transfer coefficient (m/s)
k_s	geometrical factor of the particle or of the micropore or crystal: 0 - slab; 1 - cylinder; 2 - sphere
K_{LDF}	LDF (linear driving force) coefficient: $K_{LDF} = 3D_c/r_c^2$ (s^{-1})
K_H	Henry constant (mol/kg bar)
K_i	equilibrium constant of component i (Pa^{-1})
K_i^{∞}	equilibrium constant of compound i at infinite temperature (Pa^{-1})
L	column length (m)
m_{ads}	mass of adsorbed gas (kg)
m_s	mass of adsorbent (kg)
M_W	molecular weight of the gas (kg/mol)
P	pressure (Pa)
P_0	saturation pressure (Pa)
q	absolute adsorbed phase concentration (mol/kg)
q_i	amount of adsorbate i in the adsorbed phase (mol/kg)
$q_{i,\,\max}$	specific saturation adsorption capacity of adsorbate i (mol/kg)
$\bar{q}$	crystal averaged adsorbed phase concentration (mol/kg)
$\langle\bar{q}\rangle$	particle averaged adsorbed phase concentration (mol/kg)
q^*	adsorbed phase concentration in the crystal surface (mol/kg)
r_c	micropore or crystal radius (m)
r_p	mean pore radius (m)
R_g	universal gas constant (J/mol K)
R_p	radius of the adsorbent extrudates (m)
Re	Reynolds number
Sc	Schmidt number
Sh	Sherwood number
t	time (s)
T	temperature (K)
u_0	superficial velocity (m/s)
u_i	interstitial velocity (m/s)
V_{ads}	volume of adsorbed phase (m^3)
V_c	volume of the cell where the adsorbent is located (m^3)
V_s	volume of the solid adsorbent (m^3)
y_i	molar fraction of component i
z	partition of the column length L (m)

Greek letters

Δm	difference of weight between two measurements (kg)
$(-\Delta H_i)$	isosteric heat of adsorption of component i (kJ/mol)
ε	bed porosity
ε_p	particle porosity
μ	gas viscosity (Pa s)
μ_1	first moment (s)
ρ_g	density of the gas phase (kg/m^3)
ρ_ℓ	density of the adsorbed phase (kg/m^3)
ρ_p	density of the adsorbent (kg/m^3)
σ^2	second moment (s^2)
τ_p	pore tortuosity
Ω_c	LDF (linear driving force) factor of the micropore or crystal: $\Omega_c = (k_s+1)(k_s+3)$
Ω_p	LDF (linear driving force) factor of the particle: $\Omega_p = (k_s+1)(k_s+3)$

REFERENCES

1. Draper Jr, E.L.; Beck, R. (2000) *Research and Development Needs for the Sequestration of Carbon Dioxide as Part of a Carbon Management Strategy*; The National Coal Council: , Washington, DC.
2. Ritter, J.A.; Yang, R.T. (1987) Equilibrium adsorption of multicomponent gas mixtures at elevated pressures. *Ind. Eng. Chem. Res.*, *26* (8): 1679–1686.
3. Sircar, S.; Waldron, W.E.; Rao, M.B.; Anand, M. (1999) Hydrogen production by hybrid SMR-PSA-SSF membrane system. *Sep. Purif. Technol.*, *17*: 11–20.
4. HY2SEPS. Hybrid Hydrogen Carbon Dioxide Separation Processes; European Research Project, 2005, http://hy2seps.iceht.forth.gr/
5. Baksh, M.S.A.; Ackley, M.W. Pressure swing adsorption process for the production of hydrogen. U.S. Patent 6,340,382, January 22, 2002.
6. Baksh, M.S.A.; Terbot, C.E. Pressure swing adsorption process for the production of hydrogen. U.S. Patent 6,503,299, January 7, 2003.
7. Kumar, R. Adsorption process for recovering two high purity gas products from multicomponent gas mixtures. U.S. Patent 4,913,709, April 3, 1990.
8. Le Bec, R.L. Method for purifying hydrogen-based gas mixtures using calcium X-zeolite. U.S. Patent 6,849,106, January 2, 2005.
9. Rodrigues, A.E.; LeVan, M.D.; Tondeur, D. (1989) *Adsorption: Science and Technology*; Kluwer: Boston, MA.
10. Sircar, S. Separation of multicomponent gas mixtures. U.S. Patent 4,171,206, October 16, 1979.

11. Yang, R.T. (1987) *Gas Separation by Adsorption Processes*; Butterworths: Boston.
12. Chlendi, M.; Tondeur, D. (1995) Dynamic behaviour of layered columns in pressure swing adsorption. *Gas Sep. Purif.*, *9*: 231.
13. Park, J.-H.; Kim, J.-N.; Cho, S.-H.; Kim, J.-D.; Yang, R. T. (1998) Adsorber dynamics and optimal design of layered beds for multicomponent gas adsorption. *Chem. Eng. Sci.*, *53*: 3951–3963.
14. Dreisbach, F.; Staudt, R.; Keller, J.U. (1999) High pressure adsorption data of methane, nitrogen, carbon dioxide and their binary and ternary mixtures on activated carbon. *Adsorption*, *5*: 215–227.
15. Cavenati, S.; Grande, C.A.; Rodrigues, A.E. (2006) Separation of CH4/CO2/N2 mixtures by layered pressure swing adsorption for upgrade of natural gas. *Chem. Eng. Sci.*, *61*: 3893–3906.
16. Cavenati, S.; Grande, C.A.; Rodrigues, A.E. (2004) Adsorption equilibrium of methane, carbon dioxide, and nitrogen on zeolite 13X at high pressures. *J. Chem. Eng. Data*, *49*: 1095–1101.
17. Grande, C.A.; Silva, V.M.T.M.; Gigola, C.; Rodrigues, A.E. (2003) Adsorption of propane and propylene onto carbon molecular sieve. *Carbon*, *41*: 2533–2545.
18. Nitta, T.; Shigetomi, T.; Kuro-Oka, M.; Katayama, T. (1984) An adsorption isotherm of multi-site occupancy model for homogeneous surface. *J. Chem. Eng. Jpn.*, *17*: 39–45.
19. Silva, J.A.C.; Rodrigues, A.E. (1999) Multisite langmuir model applied to the interpretation of sorption of n-paraffins in 5A zeolite. *Ind. Eng. Chem. Res.*, *38*: 2434–2438.
20. Sircar, S. (1995) Influence of adsorbent size and adsorbent heterogeneity on IAST. *AiChE Journal*, *41* (5): 1135–1145.
21. Bird, R.B.; Stewart, W.E.; Lightfoot, E.N. (2002) *Transport Phenomena,* 2nd Ed.; Wiley Imternational: Singapore.
22. Ruthven, D.M. (1984) *Principal of Adsorption and Adsorption Processes*; John Wiley & Sons: New York.
23. Yang, J.; Lee, C.-H. (1998) Adsorption dynamics of a layred bed PSA for H2 recovery from coke oven gas. *AiChE Journal*, *44* (6): 1325–1334.
24. Siriwardane, R.V.; Shen, M.-S.; Fisher, E.P.; Poston, J.A.; Shamsi, A. In: U.S. Department of Energy (Ed.), Adsorption and desorption of CO2 on solid sorbents, Carbon Sequestration - First National Conference on Carbon Sequestration, Session 3B. Capture & Sequestration III: Adsorption Studies, NETL Publications 2001.
25. Siriwardane, R.V.; Shen, M.-S.; Fisher, E.P.; Poston, J.A. (2001) Adsorption of CO2 on molecular sieves and activated carbon. *Energy Fuels*, *15*: 279–284.
26. Siriwardane, R.V.; Shen, M.-S.; Fisher, E.P. (2005) Adsorption of CO2 on zeolites at moderate temperature. *Energy Fuels*, *19*: 1153–1159.
27. Choi, B.-U.; Choi, D.-K.; Lee, Y.-W.; Lee, B.-K. (2003) Adsorption equilibria of methane, ethane, ethylene, nitrogen and hydrogen onto activated carbon. *J. Chem. Eng. Data*, *48*: 603–607.

28. Taketomo, E.; Fujiura, M. Porous materials for concentration and separation of hydrogen or helium, and process therewith for the separation of the gas. U.S. Patent 4,482,360, November 13, 1984.
29. Jee, J.-G.; Kim, M.-B.; Lee, C.-H. (2001) Adsorption characteristics of hydrogen mixtures in a layered bed: binary, ternary, and five-component mixtures. *Ind. Eng. Chem. Res.*, *40* (3): 868–878.
30. Warmuziński, K.; Tańczyk, M. (1997) Multicomponent pressure swing adsorption Part I. Modelling of large-scale PSA installations. *Chem. Eng. Process.*, *36*: 89–99.
31. Sircar, S.; Golden, T.C.; Rao, M.B. (1996) Activated carbon for gas separation and storage. *Carbon*, *34* (1): 1–12.